Supporting information for

# Trench topography in subduction zones: a reflection of the plate decoupling depth

Ritabrata Dasgupta, Nibir Mandal

Department of Geological Sciences, Jadavpur University, Kolkata, India;

**Contents of this file**

**Sections**

## S1. Topographic slope-break measurement

Previous studies showed the surface topography (elevation and depression) at convergent plate margins as a manifestation of the underlying subduction dynamics (Crameri et al., 2017; Cerpa and Arcay, 2020). Based on this basic premises, we aim to quantify the trench topography produced in our CFD model experiments. Natural trenches generally show strong trench parallel variations of their topographic patterns. To account for such heterogeneity, we chose multiple trench parallel sections to get a range of topographic parameters for a single subduction zone (Fig. S1a). To define the initial configuration of model topography, a Cartesian coordinate is set with the *x* axis ($z = 0$) to coincide with the model surface (Fig. S1b), which undergoes deformations to produce an uneven topography during subduction. We study our calculated trench topography in the light of existing subduction models and those observed in 2D cross-sections of natural subduction zones (Noda, 2016; Crameri et al., 2017; Riel et al., 2018; Cerpa and Arcay, 2020). To quantify the lateral extent of a trench depression ($W$) and its depth ($D$), we best fit the model surface topography with a polynomial function ($z = A_0 + A_1x + A_2x^2 + A_3x^3 \ldots$) to precisely locate the topographic slope breaks and maximum reliefs using the first and second order derivatives of this function. The limit of *x* in this function is set by the hinterland wall arc-high location. This algebraic manipulation is exercised to keep the polynomial functional value within a finite range. The mathematical method we apply to calculate the dip angles ($\theta$) of foreland and hinterland walls of a trench is as follows. Using a simple trigonometric relation, we find $\theta = \tan^{-1}(y/x)$, where $y = D$ (maximum negative trench relief) and *x* is the horizontal distance of $D$ from the hinterland and foreland side, respectively for calculating their corresponding slopes.

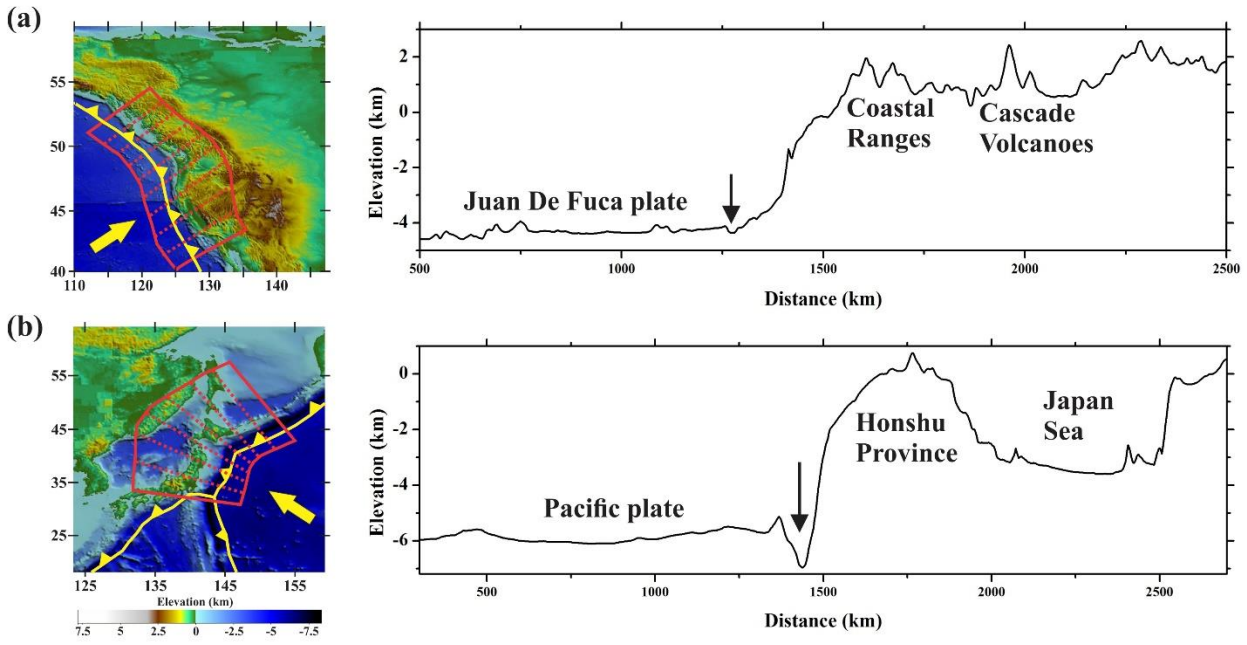


Figure S1: Digital elevation models (DEM) of (a) the Cascadia subduction zone and (b) the Northeast Japan subduction zone. Their corresponding trench normal topographic profiles are shown in the right panels. Arrows indicate the trench locations. The area marked in red lines represent the locations chosen for the topographic analysis.

## S2. Topographic stabilization after 20 Myr model run

The absolute topography of a trench in our model might increase after a model run time > 20 Myr, especially in case of MDD = 120 km. A large part of this increase results from the fore bulge growth at the boundaries of trenches. We consider the model trench depth ($D^*$) with respect to that of a far-field point in the tectonically stable topography of the subducting plate. It is found that $D^* = d^{\infty} - d_T$, where $d^{\infty}$ and $d_T$ represent depths at the far-field point and that located at the trench, measured from a horizontal reference plane (comparable to the mean sea level). The simulation experiments with varying MDD show $D^*$ approaching constant values with time (Fig. S2). Such a temporal variation of $D^*$ suggests that the model topography always tend to attain a stable state within a run time of ~ 20 Myr, especially for large MDD (> 60 km).

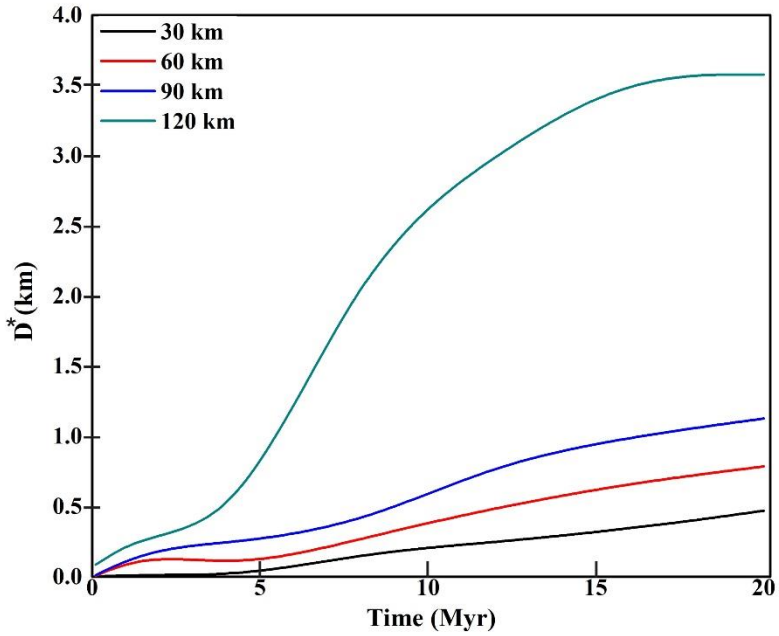


Fig. S2. Model calculated trench depths, approaching stable values with time in CFD simulations for varying MDD. $D^*$ denotes the trench depth measured with respect to the tectonically stable elevation of the subducting plate.

## S3. Low-viscosity plate margin model

We developed a model containing a low-viscosity ($10^{21}$ Pa s) zone at the plate margin, keeping MDD = 60 km. This model shows the evolution of trench, both in terms of its maximum depth and width, qualitatively similar to that produced in the equivalent model without any low-viscosity margin (Fig. S3a). The trench width evolves with nearly a constant width. The low-viscosity plate margin model allows the absolute topographic depression of the trench to increase with time, but eventually yields a value in the same order; for example, after $t$ = 20 Myr, $D$ = 1.35 km, which is 1 km in a model without low-viscosity zone. Both the models develop similar deviatoric stress patterns. The shallow regions of plate margins are dominated by tensile stress fields, whereas deeper regions by compressional stress fields (Fig. S3b).

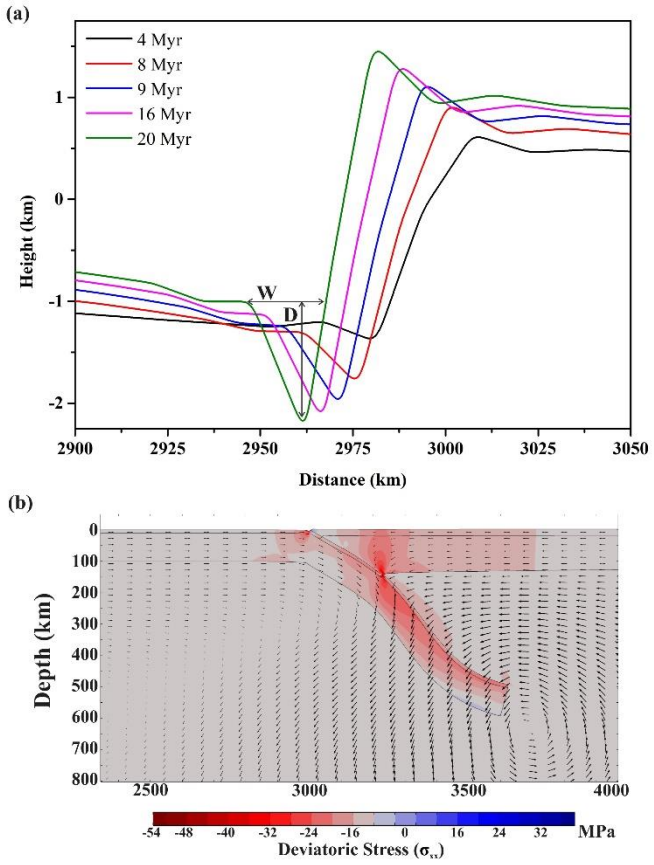


Fig. S3. (a) Time series across-trench profiles of subduction zones simulated in a MDD = 60 km model, containing a low-viscosity ($10^{21}$ Pa s) zone at the plate margin. (b) Deviatoric stress fields around the plate margin in the same model.

## S4. Constant convergence-velocity model

We ran long-time scale simulations, applying a constant (6 cm/yr) convergence velocity to the subducting plate. In these simulations we chose MDD = 60 km. The topographic profile shows strong temporal variations, and the trench yields *W* and *D* significantly lower than those produced in the spontaneous subduction model (Fig. S4). For example, after *t* = 20 Myr *W* and *D* are 15 km and 300 m respectively, which are 20 km and 1 km in the spontaneous subduction case.

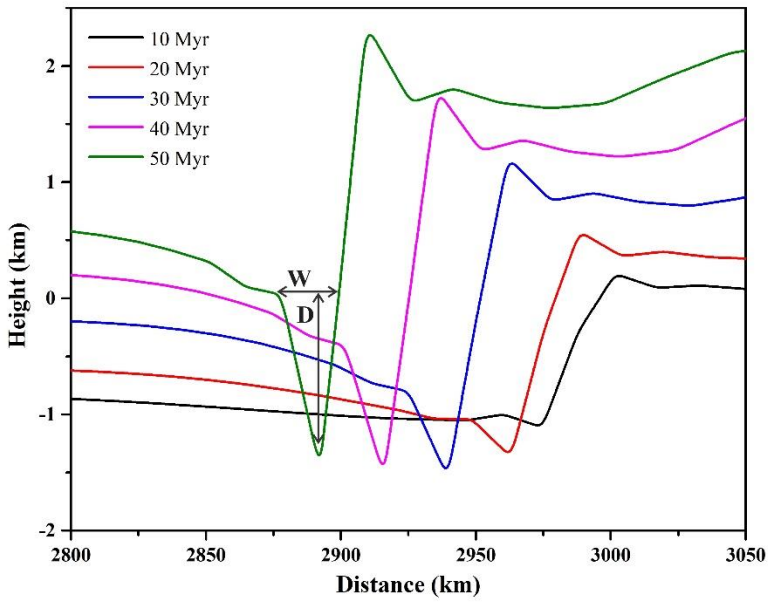


Fig. S4. Time series across-trench profiles of subduction zones simulated in a MDD = 60 km model, subjected to a constant convergence velocity (6 cm/yr) of the subducting plate.

## S5. Effects of initial model conditions on trench depth

For a better quantitative understanding of the initial model conditions on the development of trench topography, we have calculated the temporal evolutions of absolute trench depth ($D$) and $D^*$ for the experiments with 60 km MDD, with Low-viscosity plate margin ($10^{21}$ Pa s and constant convergence velocity (6 cm/yr), keeping all other parameters same. For the $D$ values, experiments with the Low-viscosity plate margin shows highest trench depth while experiments with constant convergence velocity exhibits lowest magnitude (Fig. S5a). Although the $D^*$ value suggests that all the topographies tend to stabilize and reach a steady state within the prescribed 20 Myr model run time (Fig. S5b).

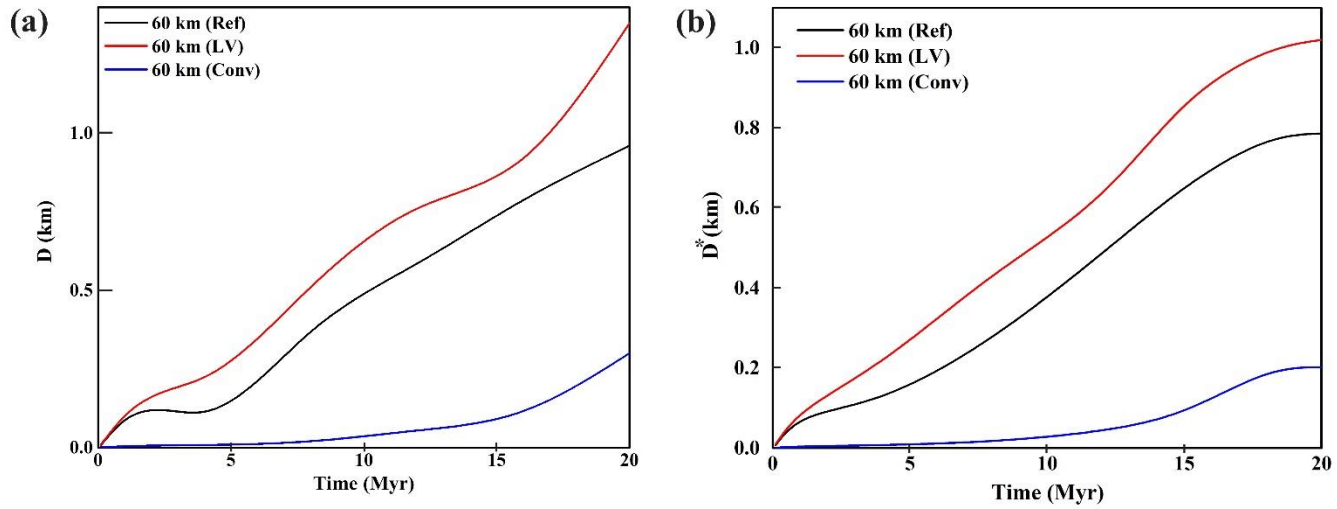


Fig. S5. Graphical plots of model calculated trench depth (*D*) for different model boundary conditions, indicated in the legend- Ref: reference simulation without any decoupling zone; LV: simulation model containing low-viscosity zone at the plate margin; and Conv: simulation model run with a constant convergence velocity applied to the subducting plate. MDD = 60 km in all the simulations.

Table S1. Model parameters used in the numerical experiments.

| Parameter | Value | Unit |
|---|---|---|
| **Length of Model** | 6000 | km |
| **Height of Model** | 2900 | km |
| **Length of SP/OP** | 3000 | km |
| **Thickness of Oceanic Crust** | 8 | km |
| **Thickness of Continental Crust** | 15 | km |
| **Thickness of SP Lithospheric Mantle** | 92 | km |
| **Thickness of OP Lithospheric Mantle** | 105 | km |
| **Thickness of Upper Mantle** | 520-540 | km |
| **Thickness of LV Layer** | 60 | km |
| **Thickness of Lower Mantle** | 2200 | km |
| **Density of SP Crust** | 3000 | $kg/m^3$ |
| **Density of OP Crust** | 2800 | $kg/m^3$ |
| **Density of SP Lithospheric Mantle** | 3240 | $kg/m^3$ |
| **Density of OP Lithospheric Mantle** | 3200 | $kg/m^3$ |
| **Density of Mantle** | 3200 | $kg/m^3$ |
| **Viscosity of Oceanic-Continental Crust** | $10^{22}$ | Pa.s |
| **Viscosity of SP-OP Lithsopheric Mantle** | $10^{22}$ | Pa.s |
| **Viscosity of Upper Mantle** | $10^{20}$ | Pa.s |
| **Viscosity of LV Layer** | $5\times10^{19}$ | Pa.s |
| **Viscosity of Lower Mantle** | $3\times10^{21}$ | Pa.s |
| **Initial subduction angle** | 30 | Degree |
| **Initial Convergence Velocity** | 2 | cm/y |

SP and OP denote Subducting Plate and Overriding Plate, respectively. LV denotes Low Viscosity. Ref. indicates the reference experiment.

175 Table S2. Measured geometrical parameters of selected natural trenches.

176

| *Subduction Name* | *Latitude* | *Longitude* | *MDD (km)* | *W (km)* | *D (km)* | *$\theta_F$ (°)* | *$\theta_H$ (°)* | *Reference for MDD* |
|---|---|---|---|---|---|---|---|---|
| *Cascadia* | *40 to 50* | *110 to 120* | *45-75* | *24-32* | *0.1-0.26* | *1.6-1.28* | *0.76-1.73* | *Cassidy and Ellis, 1993; Bostock et al., 2002* |
| *Nankai* | *31 to 34* | *137 to 140* | *55-65* | *17-23* | *0.28-0.18* | *0.12-0.78* | *0.14-1.46* | *Hori et al., 1985; Ohkura, 2000* |
| *Alaska* | *52 to 57* | *-150 to -160* | *110-120* | *41-57* | *1.8-3* | *3.54-6.58* | *5.97-10.46* | *Rondenay et al., 2008; Abers et al., 2006* |
| *Chile* | *-34 to -19* | *-73 to -71* | *115-125* | *64-80* | *2.2-3.1* | *2.35-4.37* | *5.29-8* | *Yuan et al., 2000; Bock et al., 2000* |
| *Japan* | *36 to 42* | *140-146* | *100-130* | *72-90* | *2.1-3.6* | *1.31-3.15* | *4.18-6.46* | *Matsuzawa et al., 1986; Kawakatsu and Watada, 2007* |